



HAL
open science

Comparative Analysis of Temporal Decorrelation at P-Band and Low L-Band Frequencies Using a Tower-Based Scatterometer Over a Tropical Forest

A. Hamadi, Ludovic Villard, P. Borderies, C. Albinet, Thierry Koleck, Thuy Le Toan

► **To cite this version:**

A. Hamadi, Ludovic Villard, P. Borderies, C. Albinet, Thierry Koleck, et al.. Comparative Analysis of Temporal Decorrelation at P-Band and Low L-Band Frequencies Using a Tower-Based Scatterometer Over a Tropical Forest. *IEEE Geoscience and Remote Sensing Letters*, 2017, 14 (11), pp.1918-1922. 10.1109/LGRS.2017.2731658 . hal-01799840

HAL Id: hal-01799840

<https://hal.science/hal-01799840>

Submitted on 31 May 2021

HAL is a multi-disciplinary open access archive for the deposit and dissemination of scientific research documents, whether they are published or not. The documents may come from teaching and research institutions in France or abroad, or from public or private research centers.

L'archive ouverte pluridisciplinaire **HAL**, est destinée au dépôt et à la diffusion de documents scientifiques de niveau recherche, publiés ou non, émanant des établissements d'enseignement et de recherche français ou étrangers, des laboratoires publics ou privés.



Distributed under a Creative Commons Attribution 4.0 International License

Comparative Analysis of Temporal Decorrelation at P-Band and Low L-Band Frequencies Using a Tower-Based Scatterometer Over a Tropical Forest

A. Hamadi, L. Villard, P. Borderies, C. Albinet, T. Koleck, and T. Le Toan

Abstract—Temporal decorrelation is a critical parameter for repeat-pass coherent radar processing, including many advanced techniques such as polarimetric SAR interferometry (PolInSAR) and SAR tomography (TomoSAR). Given the multifactorial and unpredictable causes of temporal decorrelation, statistical analysis of long time series of measurements from tower-based scatterometers is the most appropriate method for characterizing how rapidly a specific scene decorrelates. Based on the TropiScat experiment that occurred in a tropical dense forest in French Guiana, this letter proposes a comparative analysis between temporal decorrelation at P-band and at higher frequencies in the range of 800–1000 MHz (the low end of the L-band). This letter aims to support the design of future repeat-pass spaceborne missions and to offer a better understanding of the physics behind temporal decorrelation. Beyond the expected lower values that are found and quantified at the low L-band compared with the P-band, similar decorrelation patterns related to rainy and dry periods are emphasized in addition to the critical impacts of acquisition time during the day.

Index Terms—Repeat pass P- and L-band SAR coherences, temporal decorrelation, tower-based scatterometer, tropical dense forests.

I. INTRODUCTION

AS A CONSEQUENCE of the temporal variations that impact radar coherent backscattering, temporal decorrelation is typically characterized by the loss of coherence between repeat pass acquisitions. Leaving aside natural or human disturbances that may impact the vegetation, these changes in radar backscatter primarily originate from ecological functioning and wind motions, under the effects of varying environmental conditions. In the short term, diurnal patterns related to solar irradiance (which drives evapotranspiration and convective winds) are rather well explained and quantified by simulations based on electromagnetic modeling [1]. In the

longer term, parameterization of such models is more difficult, especially because of the difficulty in simulating cumulative or memory effects between meteorological conditions and vegetation or soil water content. Given the complexity of these phenomena characterized by their multifactorial and unpredictable nature, statistical-based methods are better suited to the analysis of temporal decorrelation. Fostered by the preparation phase of the Biomass mission [2], [3], the extensive time series (during few years) of measurements that can be sourced from tower-based experiments such as the TropiScat (see [4]–[9] and hereinafter reminded), the current AfriScat [10], or the in-development BorealScat [11] are highly relevant for this purpose, considering the added value of simultaneous measurements from the scatterometer and those related to the flux tower. However, these experiments are limited by their footprint extent (approximately 1 h) over a specific location such that the scope of the current analysis based on the TropiScat experiment, which occurred near the Paracou research station (French Guiana), is restricted to tropical forests for which short-term temporal changes are primarily driven by diurnal variations and long-term changes are driven by conditions during dry and rainy seasons (see [4], [6]). This letter also specifically focuses on the use of P- and L-bands, of which the penetration capabilities through dense vegetation are the best suited to generate the canopy height model [12]–[14] and digital terrain model from polarimetric SAR interferometry (PolInSAR) or the 3-D backscatter distribution from SAR tomography (TomoSAR) [15]. As evidenced by the extensive literature, these techniques have demonstrated strong capabilities in the P- and L-bands for use of airborne data, but their implementation in space is still hampered by temporal decorrelation if they are based on repeat-pass acquisitions.

In the case of TomoSAR processing from repeat-pass acquisitions, temporal decorrelation can generate important focusing issues [16]. Although specific processing techniques enable the minimization of such defocusing issues [17], temporal coherence below 0.8 can be considered typical below which temporal decorrelation is, for most cases, the main perturbation source. More specific and accurate thresholds should of course result from image or tomogram quality-based criteria, but as a specific example related to TomoSAR imaging of tropical forests, the Biomass mission repeat cycle during its initial TomoSAR phase has been limited to three days. This

A. Hamadi, L. Villard, T. Koleck, and T. Le Toan are with the Centre d'Études Spatiales de la Biosphère, 31401 Toulouse, France (e-mail: alia.hamadi@hotmail.fr).

P. Borderies is with the Office National d'Études et de Recherches Aérospatiales, 31055 Toulouse, France (e-mail: Pierre.Borderies@onera.fr).

C. Albinet is with European Space Agency, ESA-ESRIN, 00044 Frascati, Italy (e-mail: clement.albinet@esa.int).

design was mainly based on TropiSAR [18], [19] and the TropiScat P-band experimental results [20]. Indeed, TropiSAR airborne repeat-pass acquisitions have shown that TomoSAR and PolInSAR processing can accommodate temporal coherences of approximately 0.8 without correction, whereas the TropiScat results showed that such a level can be ensured with a temporal baseline shorter than three days at the P-band.

Bearing in mind these key figures for the design of TomoSAR or PolInSAR spaceborne missions, this letter proposes extension and comparison of the previous analysis based on the TropiScat results at the P-band with higher frequencies for an improved understanding of temporal decorrelation and investigation of future scenarios of L-band spaceborne missions operating near 1.2 GHz [21]. For these purposes, this study takes advantage of the wide-band features of the TropiScat antenna network, which acquired measurements up to 800–1000 MHz, hereinafter referred to as low L-band frequencies.

This letter begins with an overview of the experiment and data generation in Section II, including the main processing steps used to compute the temporal coherence. The comparative analysis between measurements at P-band and low L-bands is then given in Section III, considering not only seasonal effects but also several time of reference for the coherences computation, which also impact the design of spaceborne missions. Further prospects of applications are then discussed in the conclusion.

II. DATA GENERATION

A. Overview of the Experiment

Considering the previous papers [4]–[9] dedicated to the TropiScat experiment, which include a complete description of the technical features, the following paragraph simply recalls the main characteristics. Based on a network of 20 antennas, the system had fully polarimetric and tomographic capabilities. These antennas were installed close to the top of the Guyaflux tower (~55-m high), located near the Paracou research station in French Guiana [22]. The instrument unit includes a vector network analyzer (VNA) and radio frequency switch boxes that allow routing of the signal between the VNA and the specific antenna pair associated with a specific polarization (HH, HV, VH, and VV). Because the experiment was primarily focused at the P-band, acquisitions were less frequent for the low L-band (800–1000 MHz). At the P-band, acquisitions were performed every 15 min throughout the day, whereas at the low L-band the acquisitions were limited to four intervals of one hour at 12 A.M., 6 A.M., 12 P.M., and 6 P.M., with complete acquisitions cycles also spaced by 15 min. The TropiScat experiment has been in operation since the end of 2011. In this letter, the results up to the end of 2012 are exploited during the period in which the data were successfully acquired. However, due to system issues during the 2012 dry season, VV polarization data at the low L-band could not be exploited during that period. The experiment also benefitted from the environmental data acquired at the Guyaflux tower, particularly the cumulative rainfall amounts every half an hour and the averaged wind speed every minute.

In terms of meteorological data, we stress that 2012 has been rather exceptional in the sense of pronounced dry and rainy seasons. Using the Guyaflux tower rainfall measurements, a total amount of only 38 mm of rain was recorded during the 65 days of the dry period compared with 1577 mm during the 100 days of the rainy period, whereas yearly amounts range typically from 2000 to 4000 mm.

B. Procedure for Mean Coherence Derivation

We also note that the received radar signal is measured in the frequency domain and is transformed into the time domain using the inverse fast Fourier transform, resulting in impulse responses. The temporal coherence between two complex backscattering coefficients and measured at given times and can be estimated in the following manner:

$$\gamma_{pq} = \frac{\sum_{k=1}^K \sum_{i_{\min}}^{i_{\max}} S_{t1pq}^k(i) \cdot S_{t2pq}^k(i)^*}{\sqrt{\sum_{k=1}^K \sum_{i_{\min}}^{i_{\max}} |S_{t1pq}^k(i)|^2 \sum_{k=1}^K \sum_{i_{\min}}^{i_{\max}} |S_{t2pq}^k(i)|^2}}$$

where K represents the whole number of antenna pairs, k is the pair under consideration within the sum, i_{\min} and i_{\max} are the limits of the range gate, and p and q are the polarization H or V. In our experiment, we use an array antenna consisting of 20 antennas from which 16 pairs can be used to compute the coherence at a given range. To increase the number of looks, the spatial cells of the impulse responses from several antenna pairs are combined in a single complex vector for each calculation point. For the sake of simplicity, the term “coherence” is understood hereinafter as the magnitude of the complex values.

III. COMPARATIVE ANALYSIS VERSUS TEMPORAL BASELINE AND ACQUISITION TIMES FOR DRY AND RAINY PERIODS

A. Analysis Based on the Acquisition Time at 6 A.M.

Given the past studies conducted in the framework of the Biomass mission, the optimal acquisition time at 6 A.M. has been retained, considering the minimization of ionospheric perturbations and those due to convective winds. The 6 A.M. reference time is first used to compute the mean coherences for temporal baselines ranging up to 30 days, and the results are displayed in Fig. 1 for the rainy (top) and dry (bottom) seasons.

For the rainy season, the mean coherences at the P-band drop to approximately 0.8 after 1 day for HH and VV and later decrease slowly over time to reach a value in the interval [0.71, 0.72] at 30 days. The HV coherence is lower, falling to 0.75 after 1 day and decreasing slowly over time to reach a value of 0.62 at 30 days. In the case of the low L-band (dotted lines), the trend is again similar. The HH coherence falls to 0.65 after 2 days and reaches a value of 0.44 at 30 days. The HV and VV coherences are smaller than that of HH and drop to near 0.57 in two days and to 0.42 at 30 days.

In the dry season [Fig. 1 (bottom)], the trend for all cases is different, with the mean coherence loss appearing quite progressive. In the P-band case, the mean coherence

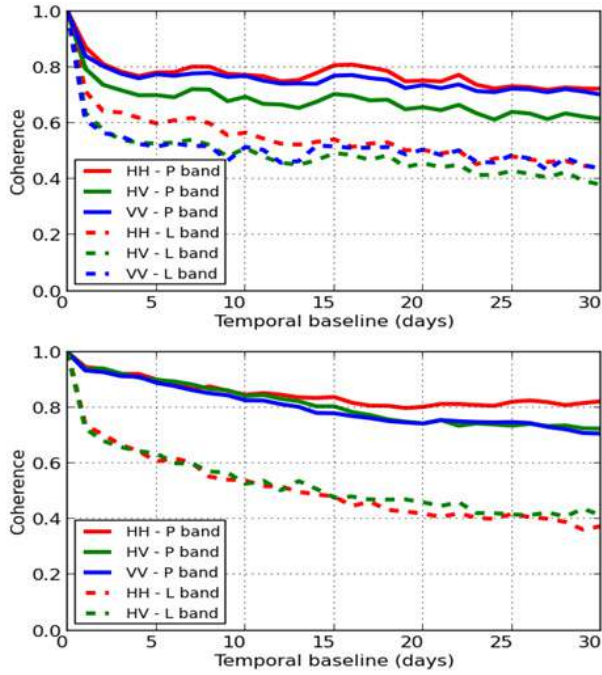


Fig. 1. Mean coherence at 6 A.M. as a function of temporal baseline for HH, HV, and VV polarizations in the case of rainy (top) and dry (bottom) periods.

decreases gradually. The HV and VV are close and rather high (still greater than 0.75 at up to 26 days). The HH is slightly higher with a value of 0.82 at 26 days. At the low L-band, the HH and HV have similar values, showing a rapid decline after one day and decreasing meaningfully until the end, reaching a value of approximately 0.4 compared with 0.82 and 0.73 at the P-band.

Comparing the P- and L-bands results in both the rainy and dry periods, it is worth highlighting these two remarks. In the rainy season, a rather rapid (as of one day) and pronounced drop is followed by a smooth decrease, whereas in the dry season the one-day drop is less severe but is followed by a linear decay with a more important slope such that as a consequence, the coherences between the rainy and dry seasons after 30 days become quite similar and actually cross each other in the low L-band case. This rather surprising result could be explained by several reasons. One reason is a possible larger range of vegetation water content (VWC) variations between the beginning and the end of a dry period compared with the rainy period, for which VWC is certainly higher but more stable. Another explanation also related to VWC could be that the attenuation becomes lower as the vegetation dries up such that the active volume that contribute to the signal is also changing, on top of possible higher probabilities of changes due to the larger number of scatterers (as reported in [23]).

B. Impact of the Acquisition Time

To further characterize the causes of decorrelation at the P- and L-bands, the effects due to changes of VWC or to wind-induced motions of the scatterers can be dissociated through the analysis of a shorter time interval. For example,

TABLE I
MEAN (μ), VARIANCE (SD^2) OF WIND VELOCITIES, AND THEIR MUTUAL RATIO DURING DRY (LEFT BLUE COLUMNS) AND RAINY (RIGHT GRAY COLUMNS) PERIODS. LINES CORRESPOND TO THE ACQUISITION TIMES CHOSEN TO COMPUTE THE COHERENCES

	μ_d	SD^2	SD^2/μ_d	μ_r	SD^2	SD^2/μ_r
12h am	2.43	0.40	0.165	2.44	1.21	0.496
06h am	2.11	0.26	0.123	2.27	1.36	0.599
12h pm	3.62	1.06	0.293	3.93	2.00	0.509
06h pm	3.34	0.75	0.224	3.10	1.38	0.445

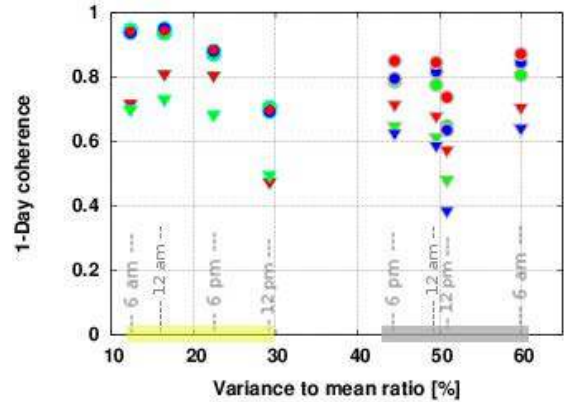


Fig. 2. Coherence after one day as a function of wind velocity variance to mean ratio. Circles and triangles, respectively, represent the P-band and low L-bands with the same color coding for polarization, and dry and rainy periods are highlighted with yellow or gray strips on the abscissa axis together with the acquisition times associated with each variance to mean ratio (explicitly given in Table I).

to study the wind effects, decorrelation at a given time of the day can be analyzed after only one day to minimize the effects of VWC changes. Table I shows the mean and variance of the wind velocity (in m/s) recorded at the tower during the dry and rainy periods. Although the mean values are comparable between periods, the variances are twice as large during the rainy period. For both periods, we also note higher values at noon or 6 P.M. compared with midnight or 6 A.M. To better isolate the effects of wind induced motions, the decorrelation values after 1 day are shown in Fig. 2, which also gathers all acquisition times and periods. With this representation as a function of the variance-to-mean ratio, one can realize the importance of the mean wind velocity and also of its variance, which lead to two separated sets of points for the dry and wet periods, respectively on the left- and right-hand sides in Fig. 2. Fig. 2 also highlights the much stronger drop at noon for decorrelation after one day.

Furthermore, considering the subsequent smoother decrease at up to 30 days, we observe first that in the rainy period case (see Fig. 3) and for both P- or low L-band cases, the overall behavior at midnight, 6 P.M. or 6 A.M. are very similar, whereas the decorrelation values at noon are much stronger but still show a rather small decrease after the one-day drop. In the dry period (see Fig. 4), the case at noon is also singular in the

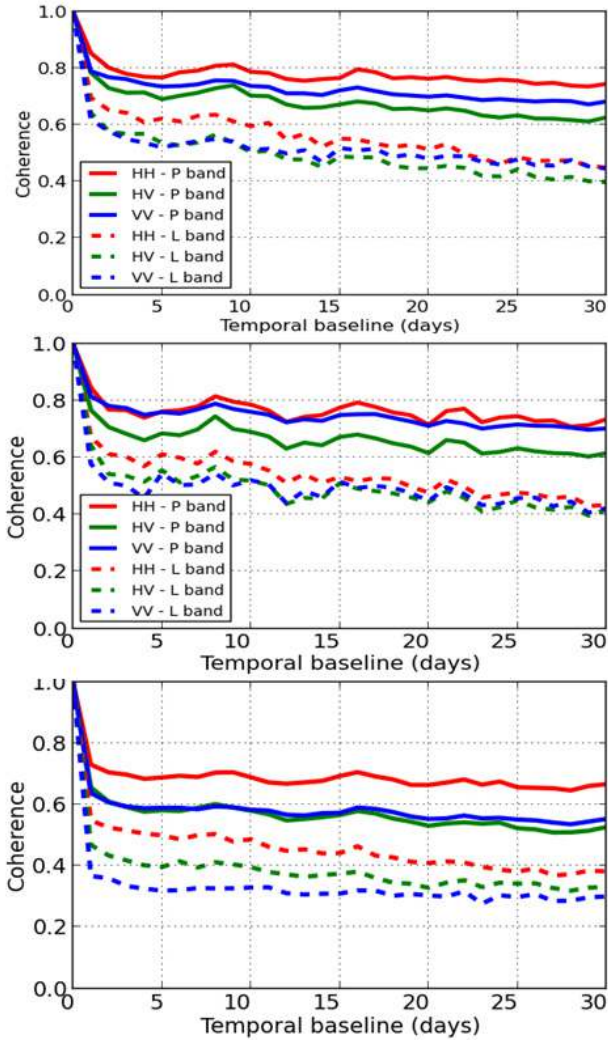


Fig. 3. From top to bottom, mean coherences versus temporal baseline for HH, HV and VV polarizations at 6 P.M., midnight and noon for the rainy period (color coding and line types are detailed in the box caption).

sense that the decrease after the one-day drop is the smallest such that the differences between acquisition times decrease with the temporal baseline, especially at the low L-band, for which all coherences become highly similar at 30 days. Apart from noon, the decorrelation curves at other times are rather similar, especially at the low L-band between midnight and 6 P.M. and at the P-band between midnight and 6 A.M., whereas 6 P.M. differs only by a stronger drop after one day.

At the low L-band, we note that the decorrelation values at midnight or 6 P.M. are less important than at 6 A.M., despite larger wind velocities. One possible explanation lies in the diurnal cycles of the VWC, which typically show a maximum near 6 A.M. in the dry period [24] but with a larger variability than the values at 6 P.M. or midnight. As a more general comment, it can be stressed that whatever the chosen reference time, the differences between the P-band and low L-bands are larger in the dry season than in the rainy season.

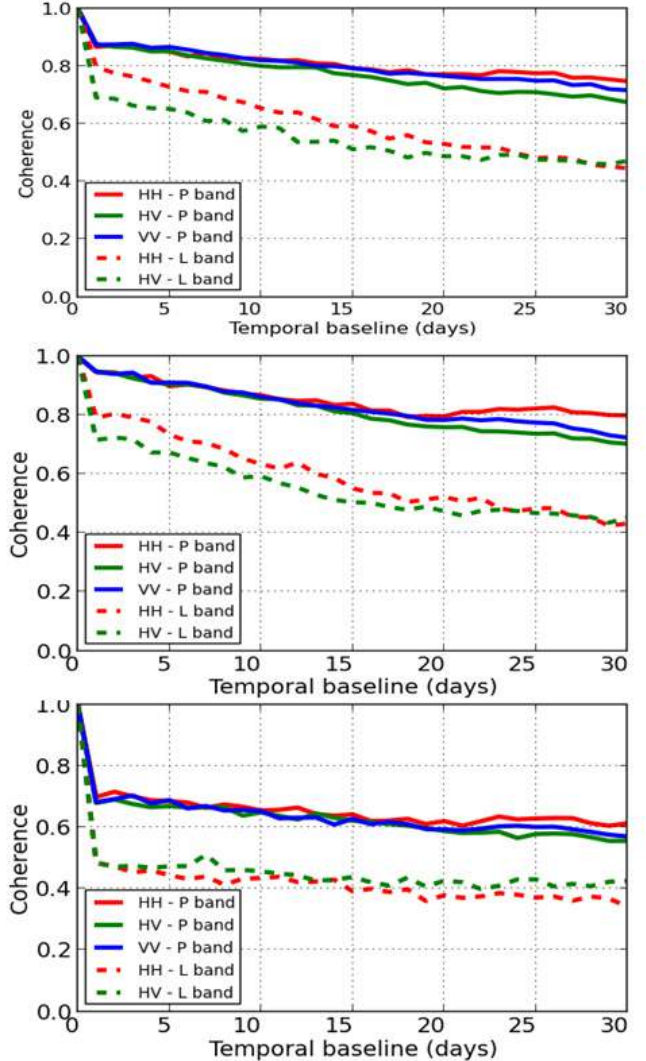


Fig. 4. From top to bottom, mean coherences versus temporal baseline for HH, HV and VV polarizations at 6 P.M., midnight and noon for the dry period.

IV. CONCLUSION

The comparative analysis in this letter shows that the low L-band decorrelation versus the temporal baseline at up to 30 days follows a similar pattern in the P-band but is more accentuated, either in terms of temporal baselines or in their magnitudes. The main insight of this letter lies in the quantification of such overall behavior due to the unique opportunity of acquiring extensive time series delivered by our flux tower-based scatterometer. The temporal decorrelation patterns at both the P-band and low L-bands differ during the dry and rainy periods, the latter being characterized by larger amount of rainfall and also by stronger and more variable winds. Either at the P- or L-band, the temporal decorrelation can be characterized by two components, a first drop after one day followed by a linear decay, the strengths of which differ significantly among the dry and rainy periods. Interestingly, a stronger decay of the linear component during the dry period can be observed such that the low L-band decorrelation at 30 days reaches the same low level of the rainy period, and the same phenomenon holds at the P-band but is delayed in time.

These results are particularly useful for the design of new spaceborne missions based on repeat-pass processing, whether to optimize the revisit period according to an acceptable decorrelation threshold or to optimize the acquisition time of the day. Considering for instance 0.8 as the value below which performances degradation can be critical without advanced specific corrections, it is worthwhile to stress that (even after only one day) our results at the low L-band are mostly not compliant with this threshold. This finding is in agreement with the development of tandem or bistatic spaceborne SAR missions [25] operating at the L-band, such as the future SAOCOM-CS mission [21] between the Argentinean and European space agencies, which would enable simultaneous interferometric acquisitions. In addition, our results at both frequencies clearly show that it is preferable to avoid an acquisition time at noon for which we observe much lower coherence values. Apart from mission planning, these quantitative results can be used in PolInSAR or TomoSAR processing steps and also offer the possibility of inferring the decorrelation at the P-band from the 0-baseline L-band observations and vice versa.

Finally, these results also create valuable data for electromagnetic models validation, which is even more consistent at several frequencies. Based on such models, further studies are expected to deepen our analysis, especially to better understand the differences between polarizations, in relation with the underlying ground topography.

ACKNOWLEDGMENT

The authors would like to thank the European Space Agency and Center National d'Etudes Spatiales (CNES) for funding of the TropiScat experiment and associated research activities, especially through the CNES research program (referred to as TOSCA). They would also like to the reviewers for their valuable comments and interest in the research topic.

REFERENCES

- [1] L. Villard, T. Le Toan, D. H. T. Minh, S. Mermoz, and A. Bouvet, "Forest biomass from radar remote sensing," in *Land Surface Remote Sensing in Agriculture and Forest*, N. Baghdadi and M. Zribi, Eds. Amsterdam, The Netherlands: Elsevier, 2016, ch. 9, pp. 363–425.
- [2] *Report for Mission Selection: BIOMASS*, document ESA SP-1324/13, European Space Agency, Noordwijk, The Netherlands, 2012.
- [3] T. Le Toan *et al.*, "The BIOMASS mission: Mapping global forest biomass to better understand the terrestrial carbon cycle," *Remote Sens. Environ.*, vol. 115, no. 11, pp. 2850–2860, Jun. 2011.
- [4] A. Hamadi *et al.*, "Temporal coherence of tropical forests at P-band: Dry and rainy seasons," *IEEE Geosci. Remote Sens. Lett.*, vol. 12, no. 3, pp. 557–561, Mar. 2015.
- [5] C. Albinet *et al.*, "TropiSCAT: A ground based polarimetric scatterometer experiment in tropical forests," *IEEE J. Sel. Topics Appl. Earth Observ. Remote Sens.*, vol. 5, no. 3, pp. 1060–1066, Jun. 2012.
- [6] A. Hamadi *et al.*, "Temporal survey of polarimetric P-band scattering of tropical forests," *IEEE Trans. Geosci. Remote Sens.*, vol. 52, no. 8, pp. 4539–4547, Aug. 2014.
- [7] T. Koleck *et al.*, "TropiSCAT: A polarimetric and tomographic scatterometer experiment in French Guiana forests," in *Proc. IEEE Geosci. Remote Sens. Symp. (IGARSS)*, Jul. 2012, pp. 7597–7600.
- [8] D. Ho Tong Minh *et al.*, "Vertical structure of P-band temporal decorrelation at the Paracou forest: Results from TropiScat," *IEEE Geosci. Remote Sens. Lett.*, vol. 11, no. 8, pp. 1438–1442, Aug. 2014.
- [9] H. T. M. Dinh *et al.*, "Ground-based array for tomographic imaging of the tropical forest in P-band," *IEEE Trans. Geosci. Remote Sens.*, vol. 51, no. 8, pp. 4460–4472, Aug. 2013.
- [10] *AfriScat Implementation Plan*, document n°4000111758/14/NL/eg, ESA Contract, 2014.
- [11] M. H. L. Ulander *et al.*, "BorealScat: A tower experiment for understanding temporal changes in P- and L-band backscattering from a boreal forest," in *Proc. ESA Living Planet Symp. (LPS)*, May 2016, pp. 9–13.
- [12] K. Florian, P. Kostas, H. Irena, and H. Dirk, "Forest height estimation in tropical rain forest using Pol-InSAR techniques," in *Proc. IEEE Int. Conf. Geosci. Remote Sens. Symp. (IGARSS)*, Jul./Aug. 2006, pp. 2193–2196.
- [13] F. Garestier, P. Dubois-Fernandez, and K. Papathanassiou, "Pine forest height inversion using single-pass X-band PolInSar data," *IEEE Trans. Geosci. Remote Sens.*, vol. 46, no. 1, pp. 59–68, Jan. 2008.
- [14] S. Solberg, E. Naesset, T. Gobakken, and O. M. Bollandsås, "Forest biomass estimated from height change in interferometric SAR height models," *Carbon Balance Manage.*, vol. 9, no. 5, Sep. 2014. [Online]. Available: <https://doi.org/10.1186/s13021-014-0005-2>
- [15] M. D. M. d'Alessandro, and S. Tebaldini, "Phenomenology of P-band scattering from a tropical forest through three-dimensional SAR tomography," *IEEE Geosci. Remote Sens. Lett.*, vol. 9, no. 3, pp. 442–446, May 2012.
- [16] G. Fornaro and A. Pauciuolo, "LMMSE 3-D SAR focusing," *IEEE Trans. Geosci. Remote Sens.*, vol. 47, no. 1, pp. 214–223, Jan. 2009.
- [17] F. Lombardini and F. Cai, "Temporal decorrelation-robust SAR tomography," *IEEE Trans. Geosci. Remote Sens.*, vol. 52, no. 9, pp. 5412–5421, Sep. 2014.
- [18] P. Dubois-Fernandez *et al.*, "The TropiSAR airborne campaign, in French Guiana: Objectives, description and observed temporal behavior of the backscatter signal," *IEEE Trans. Geosci. Remote Sens.*, vol. 50, no. 8, pp. 3228–3241, Aug. 2012.
- [19] S. Daniel, P. Dubois-Fernandez, A. Arnaubec, and S. Angelliaume, "Temporal decorrelation analysis at P-band over tropical forest," in *Proc. IEEE Int. Geosci. Remote Sens. Symp. (IGARSS)*, Jul. 2011, pp. 3947–3950.
- [20] D. H. T. Minh, S. Tebaldini, F. Rocca, and T. L. Toan, "The impact of temporal decorrelation on BIOMASS tomography of tropical forests," *IEEE Geosci. Remote Sens. Lett.*, vol. 12, no. 6, pp. 1297–1301, Jun. 2015.
- [21] *Study of L- and P-Band SAR Tomography Synergies*, document 4000112571/NL/FF/gp, ESA-ESTEC Contract, 2015.
- [22] *Paracou Guyaflux Description*. Accessed: Feb. 2011. [Online]. Available: <http://www.ecofog.gf/fr/fonctionnement/guyaflux/>
- [23] C. Thiel and C. Schmillius, "Investigating ALOS PALSAR interferometric coherence in central Siberia at unfrozen and frozen conditions: Implications for forest growing stock volume estimation," *Can. J. Remote Sens.*, vol. 39, no. 3, pp. 232–250, Jul. 2013.
- [24] K. C. McDonald, R. Zimmermann, and J. S. Kimball, "Diurnal and spatial variation of xylem dielectric constant in Norway Spruce (*Picea abies* [L.] Karst.) As related to microclimate, xylem sap flow, and xylem chemistry," *IEEE Trans. Geosci. Remote Sens.*, vol. 40, no. 9, pp. 2063–2082, Sep. 2002.
- [25] L. Villard, I. Hajnsek, K. Papathanassiou, and P. Borderies, "Pol-InSAR simulations in forest bistatic scattering," in *Proc. 7th Eur. Synth. Aperture Radar (EUSAR)*, Jun. 2008, pp. 2–5.